Comparative Study of Surface-Mounted and Interior Permanent-Magnet Motors for High-Speed Applications

Jianning Dong, *Student Member, IEEE*, Yunkai Huang, *Member, IEEE*, Long Jin, *Member, IEEE*, and Heyun Lin, *Senior Member, IEEE*

***Abstract*—This paper investigates the surface-mounted permanent-magnet (SPM) and the interior permanent-magnet (IPM) motors for high-speed applications. An SPM motor and an IPM motor are designed with the same power/speed rate and the same key dimensions. Finite-element analysis is used to compare the mechanical, electromagnetic, and antidemagnetization performances of the two motors, and lumped parameter thermal networks are involved to compare their thermal performances. It can be concluded from the comparisons that the IPM motor has comparable electromagnetic performances with the SPM motor in high-speed operations, and its costs and torque per PM weight are superior to those of the SPM motor. However, its rotor structure is not as robust and is prone to irreversible demagnetization.**

***Index Terms*—Finite-element method, high-speed permanent-magnet motors, interior permanent magnet (IPM), surface-mounted magnet (SPM).**

I. Introduction

HIGH speed permanent magnet (HSPM) motors are extensively researched for its high power density and the elimination of the brittle gearbox when driving high speed loads, e.g., compressors, blowers and expanders [1]. Generally speaking, there are two kinds of rotor topologies for the permanent magnet (PM) machines, the surface-mounted PM (SPM) one and the interior PM (IPM) one. For high speed operations, the PMs should be fixed in the rotor against the high centrifugal forces. For the SPM ones, interference fitted rotor sleeves made of high strength alloy or composite materials as shown in Fig. 1(a) are always used [2]. For the IPM ones, the conventional topology shown in Fig. 1(b) suffers from the contradiction between the rotor flux leakage and the brittle IPM bridges [3], therefore a modified spoke type IPM topology shown in Fig. 1(c) is frequently used in high speed applications.

To work out the pros and cons of the two topologies for HSPM motors and find their most suitable working conditions, this paper compares the electromagnetic, mechanical, thermal and anti-demagnetization performances of two motors with rotor topologies shown in Fig. 1(a) and (c). The weights and costs are also compared for the two structures.

Manuscript received October 17, 2015; accepted November 26, 2015. Date of publication January 4, 2016; date of current version January 19, 2016. This work was supported in part by the Natural Science Foundation of China under Project 51377019.

The authors are with the Engineering Research Center for Motion Control of Ministry of Education, Southeast University, Nanjing 210018, China (e-mail: jnd.dong@gmail.com; huangyk@seu.edu.cn; jinlong@seu.edu.cn; hyling@seu.edu.cn).

Digital Object Identifier 10.1109/TASC.2016.2514342

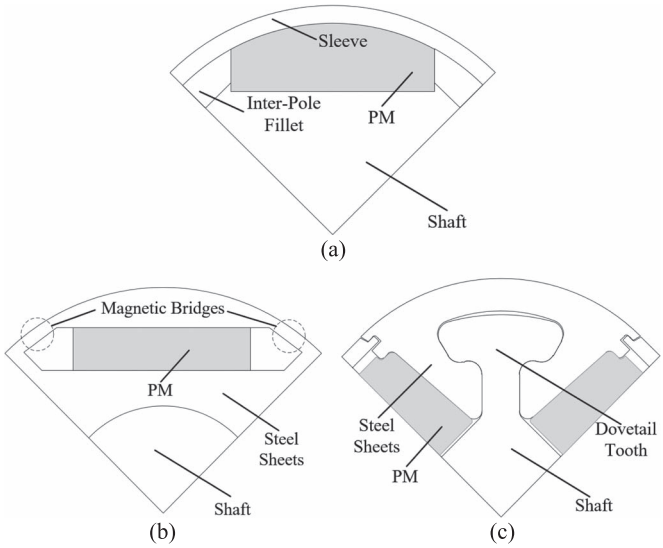

Fig. 1. Rotor topologies for PM motors. (a) SPM. (b) Conventional IPM. (c) Spoke-type IPM.

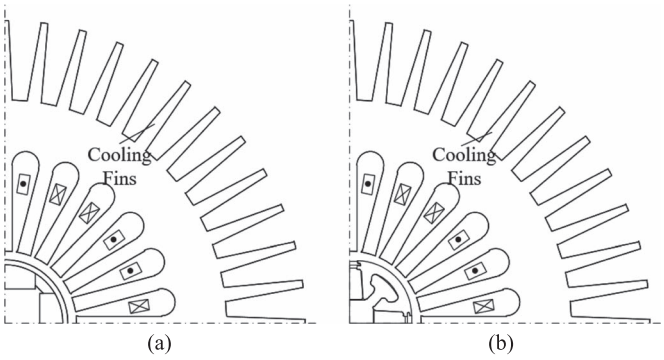

Fig. 2. Structures of the investigated motors. (a) SPM. (b) IPM.

II. Motor Structure and Parameters

The two motors investigated in this paper are both rated at 140 kW, 24 kr/min. Structures of the two motors are shown in Fig. 2. It can be seen that to enhance the stator cooling, cooling fins are punched directly on the stator laminations.

The rotor of the SPM motor is with 4 bread-shape magnets protected by a retaining sleeve made of high strength alloy Inconel 718. In the spoke-type IPM motor, the C-shaped iron laminations are mounted on the shaft with dovetail teeth, and the trapezoidal PMs are embedded between the C-shaped iron

TABLE I
MAIN PARAMETERS FOR THE INVESTIGATED MOTORS

Parameters	SPM	IPM
Stator/Rotor core material	WTG-200, 0.2 mm silicon steel sheets	
Sleeve material	Inconel 718	-
Rotor PM material	R26HE, SmCo	
Stator slot number	24	
Pole number	4	
Rotor outer diameter	88 mm	
Stator outer diameter	310 mm	
Stack length	150 mm	
Sleeve thickness	3.5 mm	-
Physical air gap length	6 mm	2 mm
Number of serial turns per phase	15	14

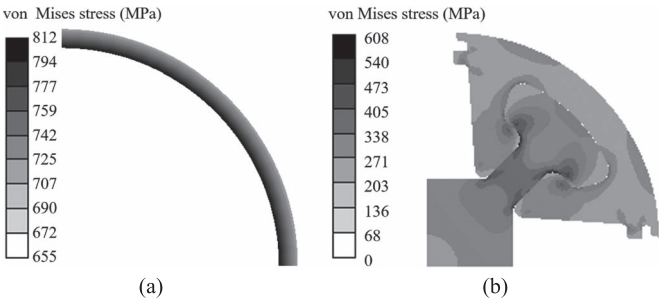

Fig. 3. FEM calculated von Mises stress distributions in the rotors under 24 kr/min, 20 °C. (a) SPM rotor sleeve. (b) IPM rotor sleeve and shaft.

laminations. The shaft is also made of Inconel 718, which is non-magnetic and can reduce the inter-pole flux leakages. Moreover, the contact area between the PMs and the rotor core is enlarged when compared with that of the conventional IPM structure, which reduces the mechanical stresses both in the PMs and the rotor core.

Main parameters of the two motors are listed in Table I. Key dimensions including the stator/rotor outer diameters, the stacking length and the slot filling factors are kept the same when designed the two motors to make the comparison fair. It can be seen from Table I that a relatively larger air gap length is used for the SPM motor to reduce the rotor eddy current loss [4].

III. ROTOR MECHANICAL ANALYSIS

Finite element analysis (FEA) is used to ensure the rotor integrity. Stress distributions under different rotating speeds and temperatures are calculated. Fig. 3 shows the calculated von Mises stress distributions in the two rotors under the rated speed and 20 °C. Calculated maximum stress and corresponding safety factors under standstill, rated speed and 1.2 times rated speed (28.8 kr/min) are listed in Table II.

As is listed in Table I, relatively large stress are induced in the SPM sleeve under the standstill conditions, which results from the interference fit of 0.15 mm between the sleeve and magnets [5]. The sleeve stress increases as the rotating speed goes up due to the increasing centrifugal force, and decreases as the rotor temperature goes down due to the higher thermal expansion coefficient of the sleeve. The maximum stress occurs at 28.8 kr/min and 20 °C, with a safety factor of 1.35. The maximum stress variation is 817 MPa to 744 MPs, i.e., 73 MPa, which is too small to induce fatigue failure.

Both the stress in the IPM rotor laminations and that in the IPM shaft goes up as the rotating speed increases. However,

TABLE II
CALCULATED MAXIMUM VON MISES STRESS (UNIT: MPA) AND CORRESPONDING SAFETY FACTORS UNDER DIFFERENT WORKING CONDITIONS

Rotor speeds (r/min)	Rotor temperature	SPM sleeve		IPM rotor			
				rotor sheets		shaft	
		stress	safety factor	stress	safety factor	stress	safety factor
0	20 ºC	798	1.38	0	-	0	-
	120 ºC	744	1.48	17.0	25.6	7.0	157
24 k	20 ºC	811	1.36	295	1.47	608	1.81
	120 ºC	760	1.45	312	1.39	585	1.88
28.8 k	20 ºC	817	1.35	413	1.05	874	1.26
	120 ºC	769	1.43	430	1.01	849	1.30

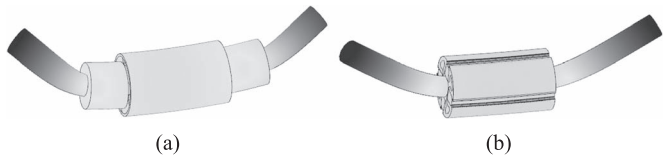

Fig. 4. First bending mode of the two rotors. (a) SPM. (b) IPM.

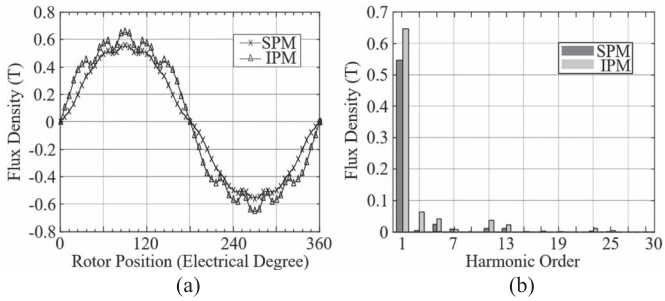

Fig. 5. (a) Calculated air gap flux density waveforms. (b) Corresponding spectra of the air gap flux density.

as the temperature goes up, the stress in the rotor laminations increases while that in the shaft decreases. Safety factors of the shaft are higher than those of the rotor laminations under all work conditions due to the higher tensile stress. The minimum safety factor is only 1.01 and the maximum stress variation is as large as 430 MPa, which means that the rotor laminations in the IPM motor are prone to break and fatigue.

Natural frequencies of the two rotors are also evaluated by using modal FEA. Fig. 4 shows the first bending modes of the SPM and the IPM rotor, corresponding natural frequencies are 1951 Hz and 1210 Hz respectively. The lamination stack in the IPM rotor has a low bending stiffness [6] while the sleeve in the SPM rotor can have some stiffening effect which results in the higher natural frequency for the SPM rotor.

IV. ELECTROMAGNETIC PERFORMANCES

Electromagnetic performances of the two motors are evaluated and compared by involving static and time-stepping circuit-coupled 2D FEA. All of the calculations in this chapter are carried out at a working temperature of 120 °C. Fig. 5 compares the flux density waveforms at the middle circle in the air gaps of the two motors. Apparently, the IPM motor has more harmonics in its air gap flux density waveform, which is caused by the rotor openings and the smaller air gap.

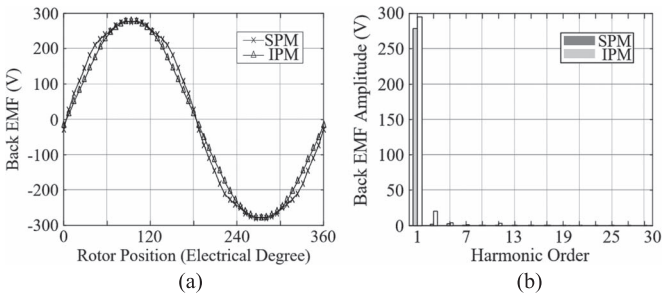

Fig. 6. (a) Calculated back EMF waveforms. (b) Corresponding spectra of the back EMF.

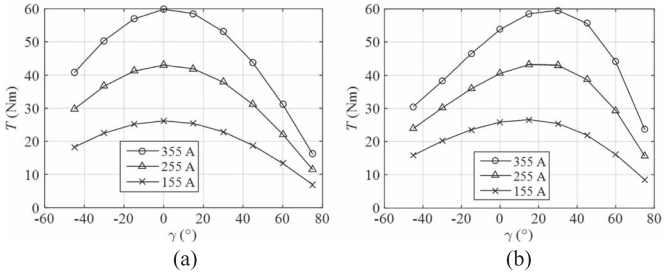

Fig. 7. $T-\gamma$ curves of the two motors under different excitations. (a) SPM. (b) IPM.

As is compared in Fig. 6, the calculated back EMF waveforms of the two motors at the rated speed are with the same amplitude. However, there are more harmonics components in that of the IPM motors, which are induced by the air gap flux density components, as is shown in Fig. 5.

Torque characteristics of the two motors are calculated by static FEA. $T-\gamma$ curves of the two motors under different armature current amplitudes are shown in Fig. 7, where T is the electromagnetic torque, γ is the angle between the armature current vector and the rotor field. It can be found that the maximum torques under each excitation are almost the same for both motors. The maximum point for the SPM is achieved at $\gamma = 0$, when the stator armature reaction field is ahead of the magnet field by 90°. The torque are pure align torque caused by the interaction between the stator and rotor fields. However, the maximum point for the IPM is achieved at $\gamma > 0$, which means that part of the armature current is allocated on the d-axis to weaken the magnet field, and the torque is composed by the align torque and the reluctance torque caused by unequal d-axis and q-axis inductances.

V. Loss and Thermal Analysis

The HSPM motors are driven by pulsed width modulated (PWM) voltage source inverters (VSIs), which may bring significant harmonic components into the stator currents [7]. These harmonics introduce extra losses both in the stators and the rotors, which give rise to temperature rises in the motors. Meanwhile, the winding resistances, magnetic performances of the magnets and the cooling coefficients of the heat dissipation surfaces are all depend on motor temperatures. Thus the driving circuits, the magnetic fields and the temperature rises of the motors are coupled together. Therefore, the loss and thermal analysis for the HSPM motors should be carried out in an iterative way.

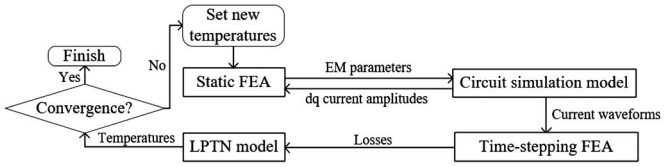

Fig. 8. Calculation flow for the losses and temperatures of the HSPM motors.

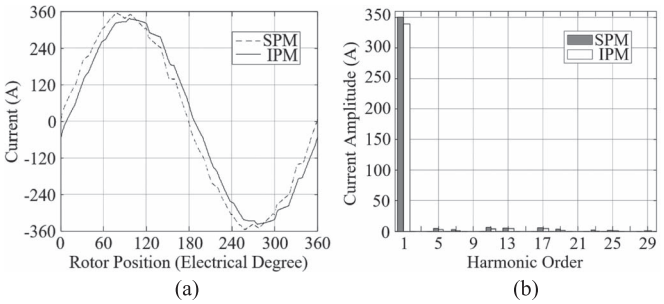

Fig. 9. (a) Simulated current waveforms. (b) Corresponding spectra of the current.

The analysis method used in this paper is shown in Fig. 8. Motor electromagnetic parameters are first calculated by using the static FEA at supposed working temperatures and dq current excitations. Then the electromagnetic parameters are substituted into the drive circuit simulation model to obtain the current waveforms for the rated output power. The substitutions between the static FEA model and the circuit simulation model are done iteratively until the variations between two adjacent calculated motor electromagnetic parameters meet a specified tolerance. Then the current waveforms are used in time-stepping FEA to calculate the motor losses. The obtained losses are set in a lumped parameter thermal network (LPTN) model to calculate the motor temperatures. The calculated temperatures are compared with the supposed temperatures to set the new temperatures. Above calculation flow continues iteratively until the temperature differences between adjacent calculations fall into the preset tolerance. The LPTN modeling techniques and temperature iteration method have been published in [4].

The two motors are both controlled by the max torque per ampere control scheme. VSIs for the two motors are both modulated by using space vector PWM. Armature current waveforms, motor losses and temperatures of the two motors under the rated conditions are calculated by the calculation flow shown in Fig. 8. The simulated current waveforms and their harmonics are shown in Fig. 9. The amplitudes of the harmonic components are slightly higher for the SPM motor when compared with the IPM ones, which is due to the lower inductances.

Copper losses are calculated by using the simulated current spectra in an analytical way presented in [8] which can consider the skin effect and the proximity effect in the winding. Iron losses and rotor eddy current losses are obtained from the FEA model, as is proposed in [9]. The calculated loss results are listed in Table III. The copper loss of the IPM motor is 20% lower than that of the SPM motor due to lower current harmonics. However, the stator iron loss of the IPM is almost 2 times higher than that of the SPM motor, which is caused by richer harmonic contents in the flux density waveforms of

TABLE III
CALCULATED MOTOR LOSSES UNDER THE RATED CONDITIONS

	SPM	IPM
Copper loss	873.4 W	694.4 W
Stator iron loss	931.7 W	2703.3 W
Rotor loss	135.7 W	197.8 W

TABLE IV
CALCULATED MOTOR AVERAGE TEMPERATURE RISES UNDER THE RATED CONDITIONS

	SPM	IPM
Stator coil	47.2 K	69.1 K
Rotor	48.0 K	53.3 K

TABLE V
PRICE, WEIGHT, AND COST OF MOTOR MATERIALS

	Price	Weight (kg)		Costs (RMB Yuan)	
	(RMB Yuan/kg)	SPM	IPM	SPM	IPM
Copper wires	58.0	17.0	15.6	986	905
Steel sheets	22.0	57.0	60.0	1254	1320
Sleeve alloy	210.0	1.2	-	246	-
PMs	250.0	2.7	1.6	675	400
Total	-	77.9	77.2	3161	2625

the IPM stator resulted from shorter air gap and non-uniform reluctances. Rotor loss of the SPM motor, which is composed by the eddy current losses induced in the rotor sleeve, magnets and shaft, is 50% lower than that of the IPM motor, which includes the iron loss in the rotor laminations and the eddy current loss induced in the rotor magnets and shaft.

Both motors are cooled by internal open-circuit air flows. The cooling air flow rates are both 10 m^3/min with an inlet temperature of 28 °C. Table IV presents calculated average temperature rises of the motor coils and rotor obtained from the LPTN model. The IPM motor is hotter both in the stator and the rotor due to more losses and shorter air gap.

VI. WEIGHT AND COST

Material costs of the HSPM motors are concentrated on the steel sheets, the rotor sleeve alloy and the enameled copper wires. Table V lists the prices, weights and costs of the materials for each motor. Apparently, the most expensive material in the motors is the rare-earth PMs. The SPM motor uses more copper while the IPM motors uses more steel, and the total weight of the two motors are almost the same. The magnets used in the IPM motor is much less than that of the SPM one. Meanwhile, the IPM motor is exempt from high strength alloy, which is considerably expensive and hard to process. Therefore, both the material costs and the processing costs of the IPM motor are much lower than that of the SPM motor.

VII. DEMAGNETIZATION RISKS

Static FEA is involved again to compare the anti-demagnetization capability for the two HSPM motors. Conventionally, the demagnetization capabilities are evaluated under the short-circuit conditions. However, since the inductances of the two motors are both too low to prevent the motor from demagnetization caused by short-circuit, the demagnetization risks are compared with an armature current vector which is 4 times of the rated one exerted on the d-axis of the FEA models.

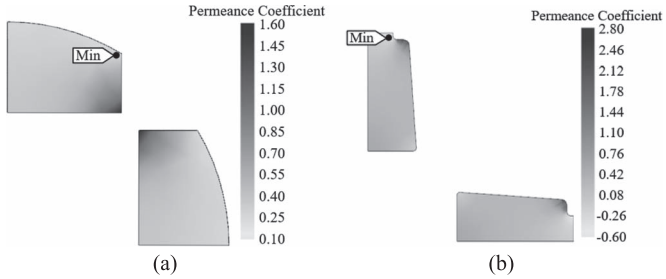

Fig. 10. Calculated permeance coefficient distributions in the PMs. (a) SPM. (b) IPM.

Fig. 10 shows the calculated permeance coefficient distributions in the PMs of the two motors. It can be seen that the permeance coefficients of the PMs in both motors are reduced to very low values. The minimum points are both located on the top corner of the PMs for both motors.

The knee point of the demagnetization curve for the SmCo PM material R26HE at 200 °C is around −0.5 T, with a permeance coefficient of −0.37. As is shown in Fig. 10, for the SPM motor, the minimum permeance coefficient is 0.16, which is much higher than the knee point, indicating that the PMs are free from irreversible demagnetization risks under the supposed working condition. However, the minimum permeance coefficient for the IPM motor is −0.54, which is far below the knee point, indicating that the PMs have been demagnetized irreversibly.

VIII. CONCLUSION

Both SPM and IPM motors are widely used in high speed applications. This paper compares the performances of the two motor structures considering their electromagnetic, mechanical and thermal performances. The motor weight, costs and the anti-demagnetization capability are also compared. Results show that the IPM motor is superior in costs while the SPM is more robust, with higher overall efficiency and cooler.

REFERENCES

[1] D. Gerada *et al.*, "High-speed electrical machines: Technologies, trends, and developments," *IEEE Trans. Ind. Electron.*, vol. 61, no. 6, pp. 2946–2959, Jun. 2014.
[2] J. Xing, F. Wang, T. Wang, and Y. Zhang, "Study on anti-demagnetization of magnet for high speed permanent magnet machine," *IEEE Trans. Appl. Supercond.*, vol. 20, no. 3, pp. 856–860, Jun. 2010.
[3] A. Binder, T. Schneider, and M. Klohr, "Fixation of buried and surface-mounted magnets in high-speed permanent-magnet synchronous machines," *IEEE Trans. Ind. Appl.*, vol. 42, no. 4, pp. 1031–1037, Jul./Aug. 2006.
[4] J. Dong *et al.*, "Electromagnetic and thermal analysis of open-circuit air cooled high-speed permanent magnet machines with Gramme ring windings," *IEEE Trans. Magn.*, vol. 50, no. 11, Nov. 2014, Art. ID 8104004.
[5] J. Dong *et al.*, "Development of an air-cooled 150 kW high speed permanent magnet motor with Gramme ring windings for turbo blowers," in *Proc. IEEE 17th ICEMS*, 2014, pp. 3534–3538.
[6] J. Lähteenmäki, "Design and voltage supply of high-speed induction machines," Ph.D. dissertation, Dept. Electr. Commun. Eng., Helsinki Univ. Technol., Espoo, Finland, 2002.
[7] L. Schwager, A. Tuysuz, C. Zwyssig, and J. W. Kolar, "Modeling and Comparison of Machine and Converter Losses for PWM and PAM in High-Speed Drives," *IEEE Trans. Ind. Appl.*, vol. 50, no. 2, pp. 995–1006, Mar./Apr. 2014.
[8] J. Pyrhonen, T. Jokinen, and V. Hrabovcova, *Design of Rotating Electrical Machines*. Chichester, U.K.: Wiley, 2009.
[9] J. Dong, Y. Huang, L. Jin, H. Lin, and H. Yang, "Thermal optimization of a high-speed permanent magnet motor," *IEEE Trans. Magn.*, vol. 50, no. 2, Feb. 2014, Art. ID 7018504.